Available online at www.sciencedirect.com
SCIENCE DIRECT
Tectonophysics 421 (2006) 145–160
TECTONOPHYSICS
www.elsevier.com/locate/tecto

Modes of thickening of analogue weak lithospheres

Florence Cagnard *, Jean-Pierre Brun, Denis Gapais

Géosciences Rennes, UMR 6118 CNRS, Université de Rennes 1, 35042 Rennes cedex, France

Received 29 July 2005; received in revised form 7 March 2006; accepted 16 April 2006
Available online 23 June 2006

Abstract

Several compressional contexts, such as those involving juvenile or thickened crust, are expected to be associated with rather hot lithospheres whose mechanical behaviour remains poorly documented. In this paper, we present a series of analogue models dedicated to compression of lithospheres characterized by a thin upper brittle crust overlying a weak ductile crust and a ductile sub-Moho mantle. The models show that (1) deformation is controlled by the ductile layers that undergo distributed thickening, (2) thrust systems are limited to the upper brittle crust, (3) thrusting induces burial and stacking of upper crust pop-downs. The overall deformation patterns can be basically interpreted in terms of pop-down thrusting of the brittle crust and pure-shear type ductile flow of crust and mantle. Moreover, the models show that the sinking of supracrustal units does not require inverse density profiles but can be simply driven by compression. Model deformation patterns are consistent with those shared by many ancient belts, including not only Archaean granite–greenstone belts, but also more generally Paleoproterozoic ones. They provide also insights on deformation modes that may characterize modern thickened and abnormally hot domains like High Plateaus.

Keywords: Compression; Weak lithospheres; Analogue modelling; Precambrian tectonics; High Plateaus

1. Introduction

The rheological layering of the continental lithosphere that is a key parameter for the dynamics of orogenic systems depends on the composition of crust and mantle, including fluids, tectonic regime and thermal state. As a first approximation one can distinguish "cold and strong" lithospheres with the highest strength located in the sub-Moho mantle from "hot and weak" lithospheres where the only high strength layer is the brittle upper crust (Brun, 2002). The transmission of compressive stresses depends directly on the presence of high strength layers. Conversely, body forces tend to be more effective in dominantly ductile lithospheres (England and McKenzie, 1982) allowing the possible development of Rayleigh–Taylor instabilities (e.g. Houseman and Molnar, 1997) or gravity collapse (Brun, 1999; Rey et al., 2001a).

Within strong lithospheres, the occurrence of a stiff sub-Moho mantle is in particular responsible for the development of lithosphere-scale thrust systems and subsequent continental subduction. This is rather well understood in modern collision zones where a décollement in the ductile lower crust allows for the subduction of the lithospheric mantle and the development of crustal-scale accretionary wedges (e.g. Alps: Schmid et al., 2004, Himalayas: Harrison et al., 1998, North American Cordillera: McClelland and Oldow, 2004, Pyrénées: Roure et al., 1989). The stacking of crustal units decoupled from the underlying lithospheric mantle has been imaged by deep seismics in several collisional belts (e.g. Choukroune, 1989; Nelson et al., 1996; Hauck et al., 1988; Schmid and Kissling,

* Corresponding author.
E-mail address: Florence.Cagnard@univ-rennes1.fr (F. Cagnard).

0040-1951/$ - see front matter © 2006 Elsevier B.V. All rights reserved.
doi:10.1016/j.tecto.2006.04.016

2000). The mechanics of stacking and crust–mantle decoupling have been explored using both analogue (e.g. Davy et al., 1990; Davy and Cobbold, 1991) (Fig. 1a) and numerical (e.g. Beaumont et al., 1996; Pfiffner et al., 2000; Braun and Pauselli, 2004) models.

In modern-type plate tectonics, soft lithospheres occur in domains of high heat flow, like back arc-type (Collins, 2002; Hyndman et al., 2005) or hot spot-type tectonic environments (Wakabayashi, 2004), or in collisional domains after significant crustal thickening and thermal relaxation, as illustrated in Tibet (Nelson et al., 1996; Clark and Royden, 2000; Mechie et al., 2004). In such tectonic environments, the Moho temperature is commonly higher than 800 °C, leading to a low strength lithospheric mantle (Sonder et al., 1987; Ranalli, 1997). In many Precambrian orogens, structural and metamorphic patterns that strongly differ from those characterizing modern plate tectonics are considered to result from deformation of soft lithospheres (Choukroune et al., 1995; Hamilton, 1998; Bailey, 1999; Hamilton, 2003; Gapais et al., 2005). A few analogue models of soft lithosphere involving a two-layer brittle–ductile crust and a wholly ductile mantle have argued for rather distributed strains, wider deformation zones, and thrust systems mainly restricted to the upper brittle crust in the absence of a brittle sub-Moho mantle, compared with strain localisation observed within 4-layer lithospheres with a high strength sub-Moho mantle (Davy et al., 1990; Davy and Cobbold, 1991) (Fig. 1b). These models bring some light on possible causes of the peculiar deformation patterns frequently observed in ancient orogenic belts where large-scale thrust systems are in particular poorly documented (Gapais et al., 2005 and refs. therein). However, despite frequent peculiarities, Precambrian orogens are often interpreted in terms of modern Alpine tectonics (Windley, 1993; De Wit, 1998). In other words, the deformation of soft lithospheres is not very well know and most often remains a matter of debate between extremely opposite opinions.

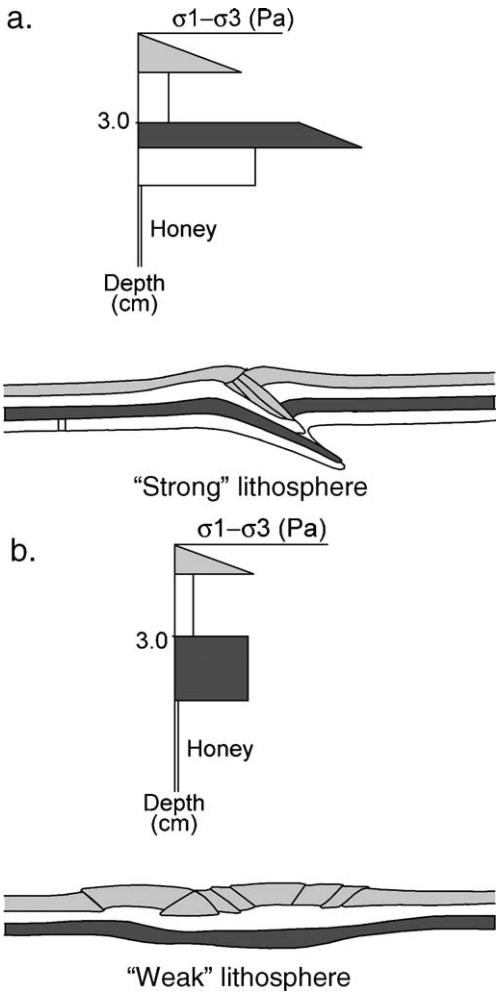

Fig. 1. Examples of lithosphere-scale analogue compressive experiments involving a brittle sub-Moho mantle (a) and a ductile sub-Moho mantle (b) (modified after Davy et al., 1990 and Davy and Cobbold, 1991).

In the present paper, we describe a series of analogue models of soft lithospheres that underwent strong horizontal compression. Models are all made of a thin upper brittle layer resting on top of two thick viscous layers representing the ductile crust and mantle. A broad range of strength profiles has been explored through experiments run at different room temperatures and shortening velocities. The deformation modes that characterise these weak lithosphere models are analysed with reference to variations in rheology. Implications are discussed with particular reference to Precambrian tectonics and to modern thickened compressive deformation zones.

2. Experimental procedure

In our experiments, a brittle–ductile slab representing a lithosphere floating on top of a low viscosity fluid representing the asthenosphere is shortened horizontally at constant velocity (Fig. 2a). We assume that the thermal state of the lithosphere at the onset of shortening is such that both the lower crust and the lithospheric mantle have a fully ductile behaviour. Consequently, the lithospheric slab is made of one sand layer to simulate a frictional upper crust and of two silicone layers with different viscosities and densities to simulate the ductile middle–lower crust and the lithospheric mantle. Our silicone putties (GS1R gum from Rhone Poulenc, France) exhibit a temperature-dependent viscosity expressed by various viscosity contrasts between the

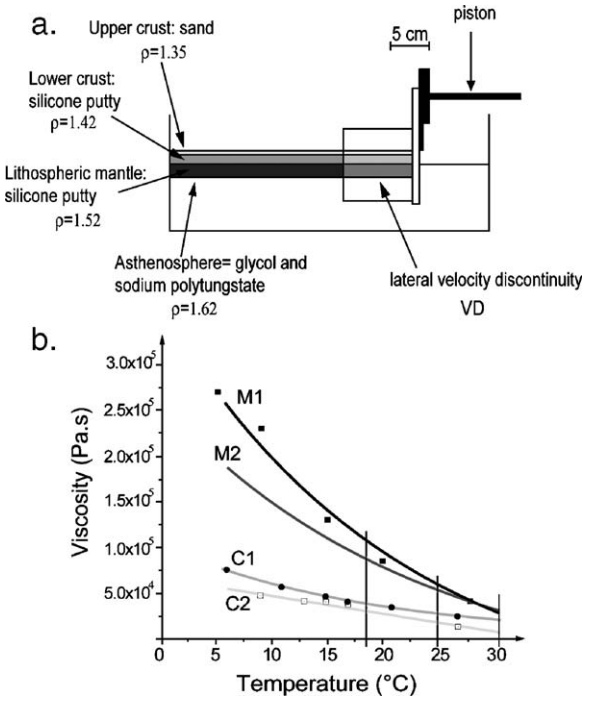

Fig. 2. Experimental setting (a) and viscosity–temperature relationships for the silicones used in the experiments (b). M1 and M2, silicones used for the mantle. C1 and C2, silicones used for the ductile crust. Vertical lines indicate the three temperatures tested in the series of experiments.

ductile crust and the ductile mantle within a 20 °C temperature range (Fig. 2b). The scaling of comparable lithosphere-scale models has already been discussed in several previous papers to which the reader is referred for details (e.g. Davy and Cobbold, 1991; Brun, 2002).

We present five experiments with identical initial geometry and physical properties but with variable boundary velocity (V) and room temperature (T). By varying these two parameters, one can examine the impact that contrasted coupling between the various lithospheric layers has on the deformation mode. Indeed, an increase in model shortening velocity results in a decrease in the relative strength between brittle and ductile layers. Running experiments at different room temperatures allows further exploration of the impact of strength contrasts between silicone layers on deformation modes (Fig. 2b). The strength profiles for the five experimental runs are given in Appendix 1.

2.1. Analogue materials

The upper crust is made of dry Fontainebleau sand, a cohesionless eolian quartz sand with a frictional angle of about 30°. Its density was adjusted to 1.35 by adding ethyl-cellulose powder. Newtonian silicone putties (GS1R gum from Rhone Poulenc, France) with densities of 1.42 and 1.52 are used to represent the ductile crust and mantle, respectively. Their viscosities vary with temperature between 3.0×10^5 and 5.0×10^4 Pa s (Fig. 2b and Table 1). The initial thickness of the different layers was fixed to 0.5 cm for the upper brittle crust, 1 cm for the ductile crust, and 1.5 cm for the lithospheric mantle. In order to introduce markers within the models, the ductile crust and mantle layers are made of silicone sub-layers of different colours that display a slight contrast in viscosity (Fig. 2b and Table 1).

A low viscosity fluid made of a mixture of glycol, water and sodium polytungstate, with a density adjusted to 1.62, represents the asthenosphere.

2.2. Deformation rig

The model is set up in a rectangular tank ($40\times30\times12$ cm) inside which a mobile wall connected to two half-side walls and driven at a constant rate by a screw jack powered by a stepping motor (Fig. 2a). The free extremity of each of the half-side walls imposes velocity discontinuities (VD) within the model. This was made in order to favour strain localization away from the moving plate.

Table 1
Physical parameters for the different experiments performed

Temperature T (°C)	Velocity V (cm/h)	Viscosity μ (Pa s)				Mean viscosity contrast	Mean viscosity difference (Pa s)
		Crust		Mantle			
		C1	C2	M1	M2		
30	5.0	2.2×10^4	1.00×10^4	4.00×10^4	3.40×10^4	2.31	2.10×10^4
	1.0						
	0.5						
25	0.5	2.50×10^4	1.50×10^4	5.50×10^4	5.50×10^4	2.75	3.50×10^4
18	0.5	3.75×10^4	2.90×10^4	1.10×10^5	9.00×10^4	3.01	6.68×10^4

2.3. Experiments

Experiments have been carried out at three constant displacement velocities of the mobile wall of 0.5, 1.0 and 5.0 cm/h and three constant room temperatures of 18, 25 and 30 °C (Table 1). In all experiments, models were shortened up to 50%. Surface photographs were taken at regular time intervals during experiments and topographic maps of model surface were acquired at different times using a laser beam scanning system.

At the end of experiments, the model surface was covered by a neutral sand layer and wetted. The model was then frozen at about −20 °C, and the asthenosphere-like fluid removed as the presence of glycol prevents freezing. The overlying frozen lithosphere slab was extracted and serial sections were sawed parallel to the shortening direction and photographed.

Main limitations of sand–silicone analogue modelling are attached to model size that must remain limited, and to the impossibility to take into account changes in rheological profiles due to thermal variations during deformation (see review in Brun, 2002). In addition, neither erosion nor sedimentation has been considered.

3. Results

3.1. Surface evolution of models

During shortening, the upper sand layer is affected by folding and reverse faulting at one or several locations depending on the applied boundary velocity and room temperature. Surface photographs (Fig. 3) and topographic images (Fig. 4) of one model (V=0.5 cm/h and T=30 °C) illustrate an example of progressive development of anticline or syncline structures associated to thrust faults.

Fault spacing is generally large (Fig. 3), defining wide undeformed domains between sites of localized deformation.

The first thrust that develops is connected to the lateral velocity discontinuities (VD) (Fig. 3a). New faults can however develop at other sites not directly controlled by the VDs (see Fig. 3b, c). In all experiments, the vergence of thrusts is strongly variable in space and time (Fig. 3), and a well-defined dominant thrust vergence was never observed. However, one common type of elementary thrust structure that developed in all experiments consists in conjugate faults bounding pop-down blocks of upper crust (e.g. PD in Fig. 3b, c).

The topographic images (Fig. 4) show that topographic highs are located close to the localized zones of faulting and that undeformed domains have not undergone significant flexure and even uplift. More generally, all models display limited relief development. This contrasts with four layer-type models (Davy et al., 1990; Davy and Cobbold, 1991) (Fig. 1a) where the lithospheric mantle contains a high strength brittle layer.

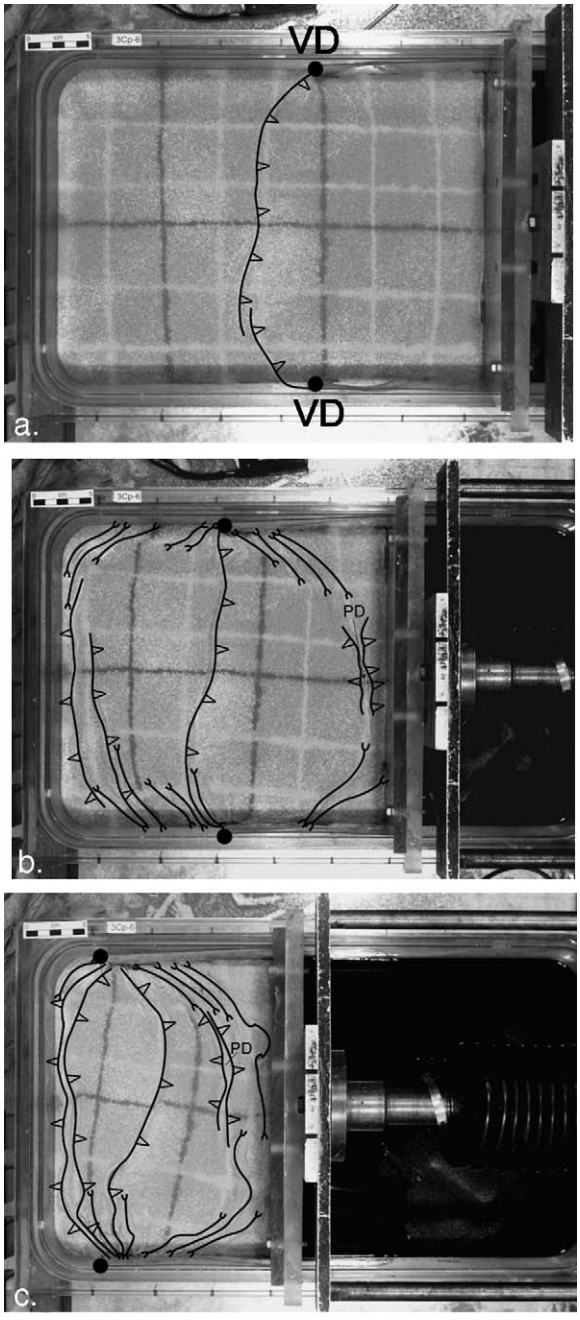

Fig. 3. Surface photographs of three successive shortening stages (10, 25 and 50%) of one experiment performed at T=30 °C and V=0.5 cm/h. Model width is 30 cm. VD are locations of lateral velocity discontinuities. Main thrusts and fold traces are underlined. PD shows location of one pop down system.

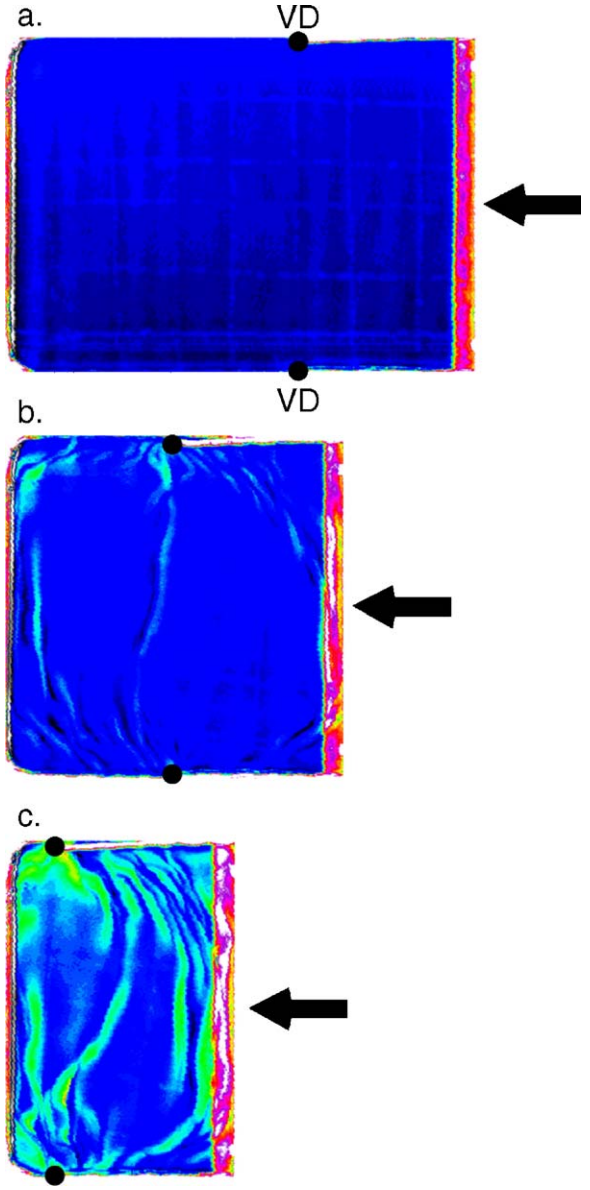

Fig. 4. Topographic maps of model shown on Fig. 3 before deformation (a) and for two successive shortening stages (25 and 50%) (b, c). Blue areas correspond to zones of no uplift or flexure. Green and yellow narrow zones correspond to main thrusts.

3.2. Fault patterns

At a constant room temperature of 30 °C, deformations change from strongly localized for low V values (Fig. 5a) to rather distributed with increasing V values (Fig. 5b, c). In all models, the pattern of faulting is dominated by a "pop-down" style leading to the incorporation of blocks of the upper brittle layer within the underlying ductile layer (Fig. 5).

Model building may lead to slight variations in the thickness of the sand layer (less than 1 mm) across models and from one model to another. Because of these slight variations in the thickness of the sand layer, the shape of pop-down structures ranges from sharp triangles (Fig. 6a) to rounded pods (Fig. 6b, c). Serial sections across one model (Fig. 5c) show the lateral variation of an isolated pop-down structure (Fig. 7). Thrust geometry and vergence changes along strike, passing from a single thrust dipping left (Fig. 7b, c) to a more symmetrical pattern (Fig. 7d), and then to an asymmetrical conjugate thrust pattern with the dominant fault dipping right (Fig. 7e, f). These serial sections also illustrate the time sequence leading to the isolation of a pop-down structure and its incorporation within the underlying ductile layer.

Fig. 8 illustrates possible successive steps leading to pop-down stacking during progressive shortening of models. During a first stage, the deformation pattern is symmetrical (Fig. 8a). Two thrusts with opposite vergence delimitate a triangular block 1 that is pushed down inside the ductile layer (Fig. 8b). This stage ends when the two conjugate thrusts meet each other. As shortening proceeds, only one thrust can remain active and the fault

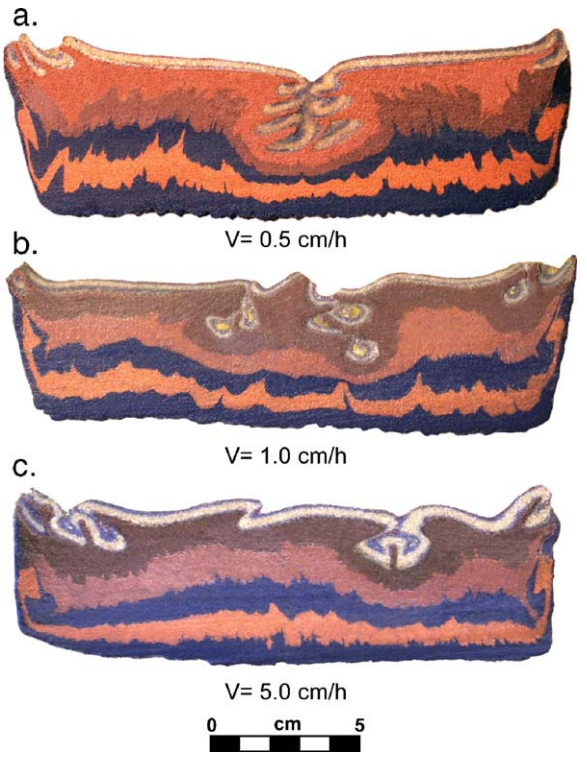

Fig. 5. Sections across the central part of three different models performed at constant T=30 °C and velocities of 0.5 cm/h (a), 1 cm/h (b) and 5 cm/h (c). Top of the uppermost blue layer is the Moho.

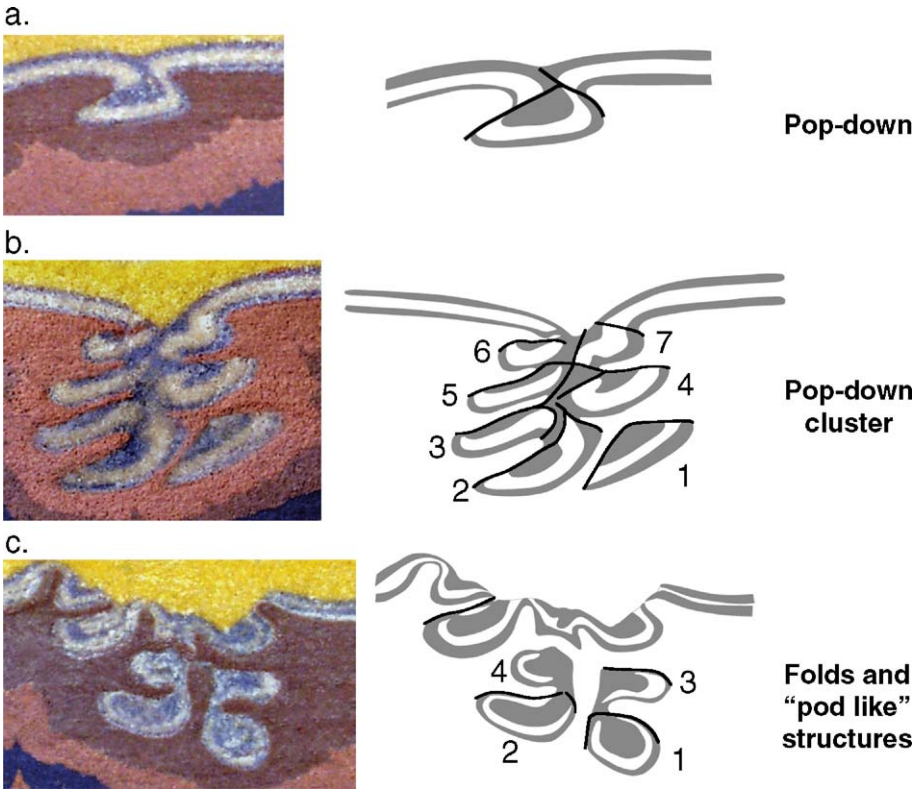

Fig. 6. Cross-sections and corresponding line drawings showing main types of pop down morphologies. Numbers refer to the order of successive pop down formation and burial. See text for further explanations.

system becomes asymmetrical (Fig. 8c). Then, a new thrust initiates and defines a block 2 that moves down together with block 1 (Fig. 8d). When the two faults controlling block 2 meet each other, a new block 3 is created (Fig. 8e). This process goes on, alternating new faults and blocks from right to left (Fig. 8f). For large amounts of shortening and provided that deformation remains localized at a single site, a crustal-scale vertical block cluster develops (Fig. 6b, c).

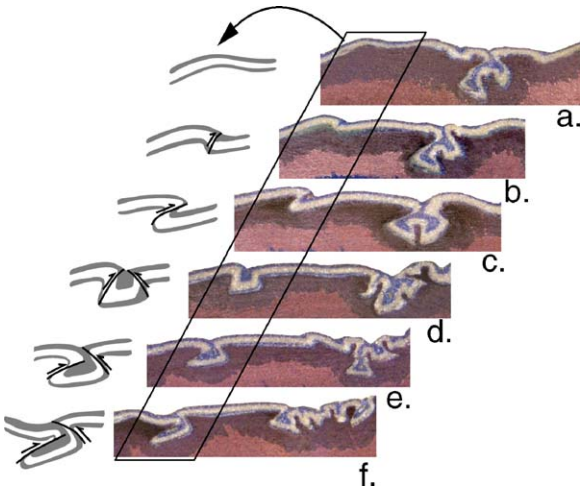

Fig. 7. Serial cross-sections and line drawings showing an example of along-strike variations of a pop down system, illustrating the way a pop down may evolve in time.

Sharp triangular fault blocks develop in experiments with thickest sand layers (Fig. 6a). In contrast, if the sand layer is slightly thinner (less than 1 mm), local shortening occurs through smooth flexure of the sand layer, evolving into synclines whose limbs join each other to form pod like structures (Fig. 6c). Despite this structural difference, the upper crust pods are incorporated into the ductile layer according to a process similar to that described in Fig. 8.

3.3. Ductile deformation

All cross sections display short wavelength folding of the interfaces between silicone putties of various colours representing the ductile crust and mantle (Fig. 5). The resulting cuspate-shape folds come from buckling instabilities due to small but significant rheological contrast between layers (Table 1) (Fig. 2b). Because the horizontal finite shortening is large (50%), folds have short wavelength and large amplitude. The

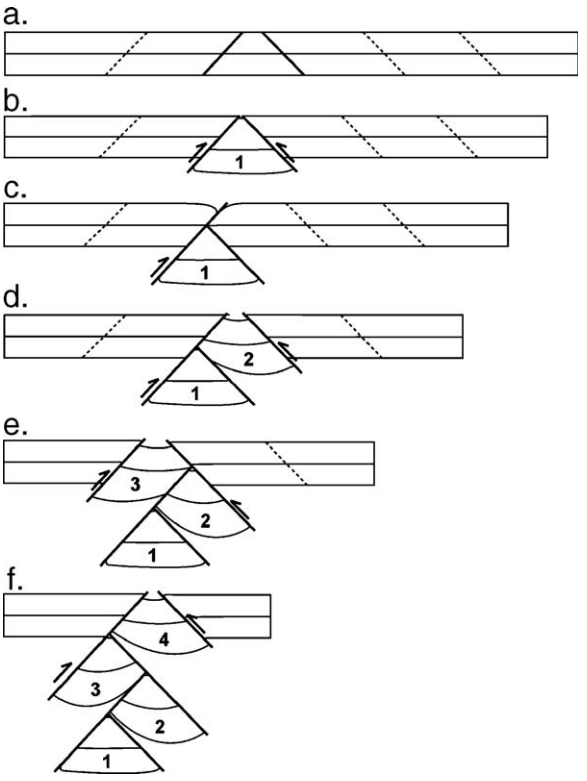

Fig. 8. Interpretative sketch of formation and evolution of a pop down cluster. Numbers refer to the order of successive pop down formation and burial. See text for further explanations.

largest folds initiate around vertically rising air bubbles that were trapped in the silicone putties during model preparation. The trajectories of the principal shortening plane $\lambda_1\lambda_2$ were deduced from the axial surface of folds (Fig. 9a, b).

To estimate the vertical component of finite strain within ductile layers, the mean envelope of the different silicone layers has been drawn on one representative deformed cross section. The ratio of layer thickness after and before deformation has been calculated throughout the cross section for each silicone layer. Contours of this vertical strain ratio (Fig. 9c) show that ductile layers in most of the model has undergone a mean thickening value of about 1.5 except a domain of vertical thinning in both crust and mantle below the block cluster (Fig. 9c). Folds affect the layer interfaces within the overall thinned area (Fig. 9a). Some of them might result from bubble tracks, but the smaller folds likely represent remnants of an early stage of horizontal shortening.

To confirm the existence of a domain of vertical shortening below the block cluster, one additional experiment was performed, with the same experimental parameters than the model of Fig. 9 but with vertical markers in the silicone ductile model-crust (Fig. 10a). Changes in marker widths underline (1) a local downward increase in the amount of horizontal shortening below the undeformed sand layer (e.g. zone A on Fig. 10a), and (2) a strong vertical shortening at the base of the block cluster (zone B on Fig. 10a). The overall curvature of vertical markers illustrates the flow pattern around the descending blocks (Fig. 10b). Despite the bulk horizontal shortening at model scale, upper-crust block burial induces a divergent flow of the underlying ductile crust and mantle. This results in a horizontal shearing top to model centre at the brittle–ductile interface (Fig. 10b). These observations explain why $\lambda_1\lambda_2$ trajectories are nearly vertical close to lateral model borders and curve around the block cluster at the centre of the model (Fig. 9b).

Fig. 11 summarizes, in cross-section, the overall pattern of $\lambda_1\lambda_2$ trajectories deduced from the combined analysis of experiments shown on Figs. 9 and 10. The domain of flat lying trajectories below the block cluster implies the existence of a neutral surface that should migrate downward during progressive stacking of pop down blocks. With increasing shortening and block stacking, the neutral surface should thus migrate from the crust to the mantle (Fig. 11). The downward migration of the neutral surface may explain why some small folds at the layer interfaces are still present in a domain that displays overall vertical shortening. These folds represent an early stage of horizontal shortening not entirely erased by subsequent vertical shortening.

One remarkable feature of the strain pattern is that, underneath an undeformed brittle upper crust, coaxial shortening affects both the ductile crust and mantle surrounding the block cluster.

3.4. Variations of structures with temperature and boundary velocity

Experiments with similar materials and initial model geometry have been carried out for room temperatures T=18, 25 and 30 °C and boundary velocities V=0.5, 1.0 and 5.0 cm/h. Because variations of T and V have direct consequences on the initial strength profiles (Appendix 1), the different models display significant differences in deformation patterns (Fig. 12). The most localized deformation pattern is observed for T=30 °C and V=0.5 cm/h. A decrease in T or an increase in V result in more distributed deformations due to an increase in the bulk strength of ductile layers, and therefore of the bulk lithosphere. Because the strength of the sand layer is independent of T and V, these strength changes also correspond to a decrease of the brittle–ductile stress ratio.

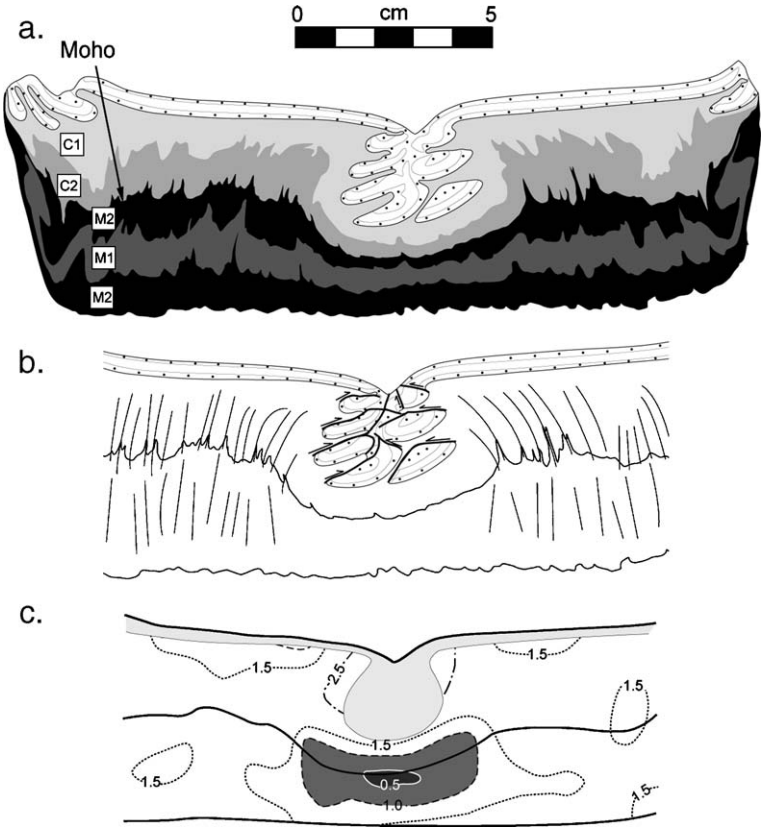

Fig. 9. (a) Line drawing of model cross-section shown in Fig. 5a (T=30 °C, V=0.5 cm/h). (b) Corresponding strain trajectories deduced from axial traces of minor folds. (c) Contours of ratios between initial and final ductile layer thickness (bulk finite vertical stretch, >1; Bulk finite vertical thinning, <1). Dark grey domains are domains of bulk finite vertical shortening beneath the pop down cluster (light grey).

All models display the same deformation process marked by (1) distributed shortening of the ductile layers, and (2) development and burial of upper crust pop downs. In all experiments, the envelope of the surface and that of the base of the model lithosphere remain rather flat. The only significant difference relates to the degree of strain localization within the brittle upper crust. When the shortening of the upper crust is strongly localized (e.g. Experiment with T=30 °C, and V=0.5 cm/h in Fig. 12), the crust displays heterogeneous thickening and the Moho shows significant deepening below the block cluster. However, away from it, the Moho envelope is flat lying. In contrast, when the shortening of the upper crust is more distributed (e.g. Experiment with T=18 °C and V=0.5 cm/h in Fig. 12), the topography of the Moho displays undulations with smaller amplitude and wavelength and therefore a rather flat envelope. With decreasing strain localization in the upper crust, the thickening of the ductile lithosphere becomes more homogeneous and domains of local vertical shortening below upper crust pop downs tend to disappear (Fig. 13).

Despite significant variations in the depth of the Moho, the base of the lithosphere remains rather flat (Fig. 12). This means that during deformation, any thickness heterogeneity created by shortening in the brittle crust is immediately compensated by lateral ductile flow to maintain a constant overall lithosphere thickness. Easy lateral flow is favoured by an extremely small strength ratio between the ductile layers and the upper crust. Moho undulations are due to density differences between the brittle upper crust, the ductile middle–lower crust and the ductile mantle. In overall, deforming models permanently trend toward isostatic equilibrium.

4. Discussion

4.1. Mechanical significance of pop-down clusters

In nature, pop-downs and pop-down clusters associated with shortening and “thrusting” as observed in our experiments appear rather unusual at crustal-scale. However, similar but smaller structures have been

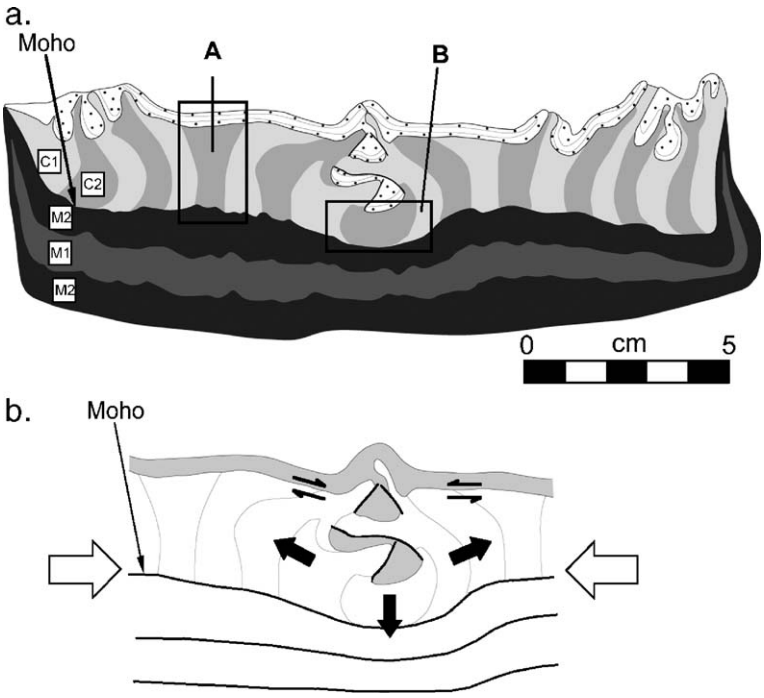

Fig. 10. (a) Cross-section through the central part of a model built with vertical markers within the ductile crust. T=30 °C and V=0.5 cm/h, similar to model Fig. 9. (b) Interpretative sketch showing main displacement directions within silicones (thick black arrows) and shear components at the brittle ductile interface. White arrows indicate the bulk shortening direction.

described in the context of salt tectonics (Brun and Fort, 2004; Fort et al., 2004). This suggests that compressional patterns observed in salt tectonics, in particular from 3D seismics, could provide useful structural data bases for application to compression of soft lithospheres. Comparable geometries may also be found at larger scale in compressive intra-mountain ramp basins bounded by conjugate thrusts with opposite vergence (Cobbold et al., 1993; Burg et al., 1994). Deformation features developed in our weak model lithospheres reflect a strong mechanical control by the ductile layers, with potential decoupling between brittle and ductile crust, as discussed below.

In compression, frictional models, as well as brittle–ductile models involving a strong sub-Moho mantle, generally lead to the building of asymmetric pop-up structures above major thrusts (Malavieille, 1984; Beaumont et al., 1996), a feature well documented in natural examples in the Pyrenees (Choukroune et al., 1990) and the Alps (Pfiffner et al., 2000). In contrast, our models with their thin and brittle layer overlying thick, ductile and weak ones provide favourable mechanical conditions for the development of rather symmetrical structures. Many works have consistently argued that high brittle–ductile ratios favours the development of thrust stacks; whereas more symmetrical thrust systems develop at lower brittle–ductile ratios (see Jackson and Talbot, 1994 and refs. therein). In our models, the strength of the ductile crust and mantle, as well as the low brittle–ductile ratios, also favour downward motion of upper-crustal blocks. As upper crust pieces have a limited thickness, room can be easily made in the ductile layers underneath. Moreover, it is noteworthy that pop-up-type structures are quite uncommon in our experiments and remain of

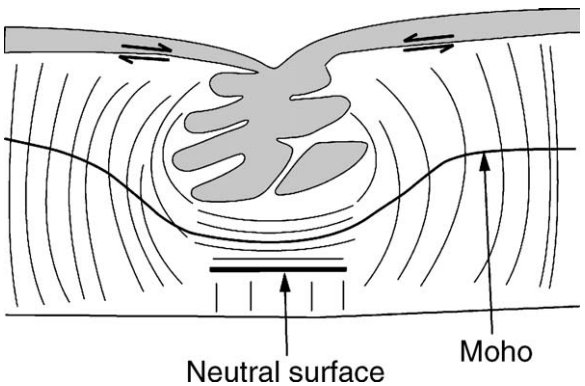

Fig. 11. Sketch summarizing main structural features associated with a pop down cluster. Steeply dipping lines are strain trajectories. See text for further explanations.

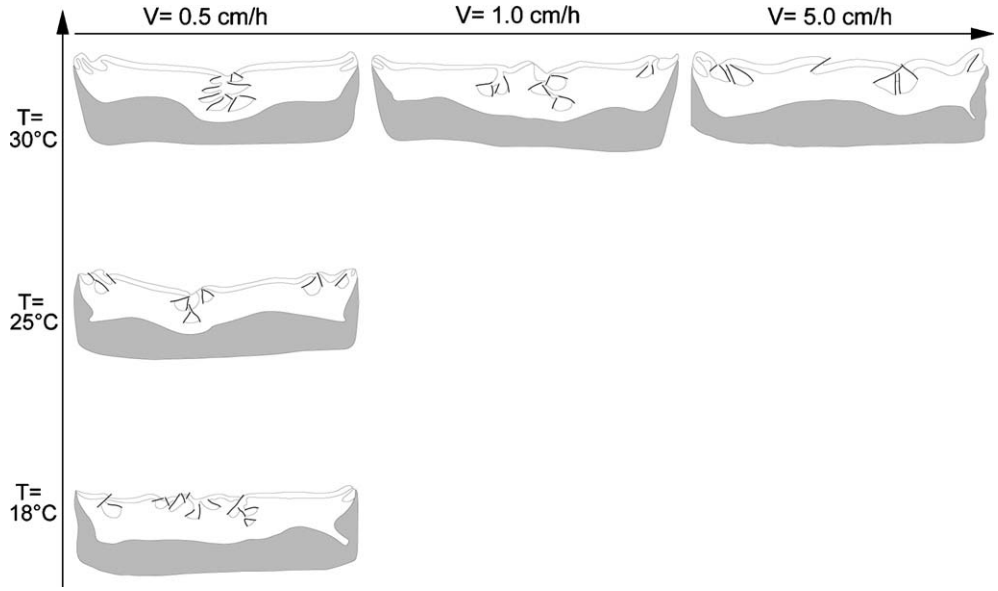

Fig. 12. Line drawings of cross-section in the central part of models deformed at different temperatures (T) and shortening velocities (V). Decrease in V or increase in T result in an increase of strain localisation in the brittle layer. Grey area is lithospheric mantle.

limited amplitude. An important consequence of the particular mechanical properties of models is that topographic highs remain localized despite an overall doubling of the thickness of the ductile lithosphere throughout models. In other words, large bulk shortening results in model surfaces that suggest rather limited strains.

4.2. Implications for Precambrian tectonics

Several features developed in our models are quite comparable to structures typically found in many ancient compressive belts involving juvenile crust and associated with high geotherms (Fig. 14). These are in particular (1) a rather distributed crustal shortening

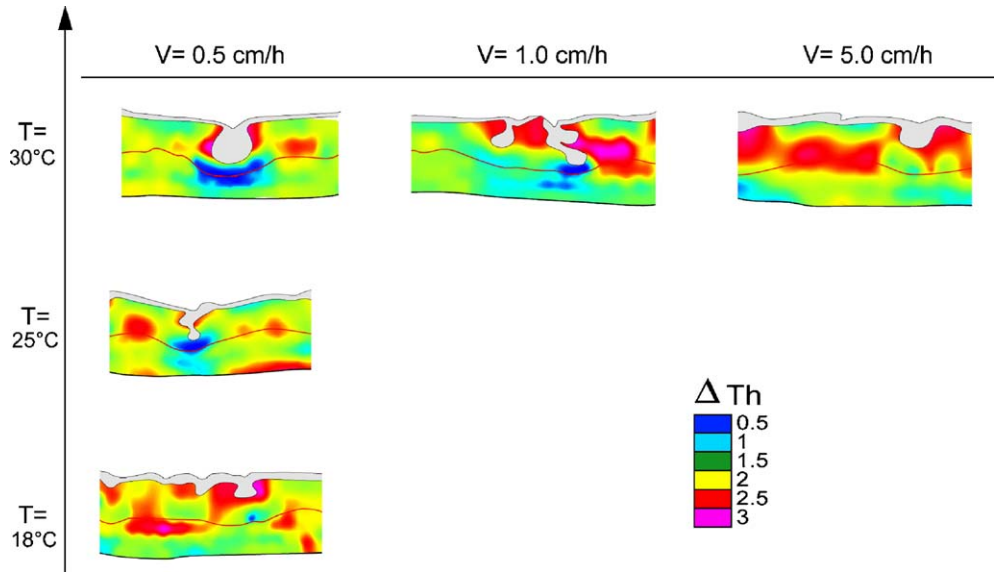

Fig. 13. Cross-sections showing variations in ratios between initial and final ductile layer thickness (bulk finite vertical stretch, >1; Bulk finite vertical thinning, <1) in central parts of models deformed at different temperatures (T) and shortening velocities (V). Red lines underline the Moho, light grey areas are sand dominated zones. Same models as in Fig. 12.

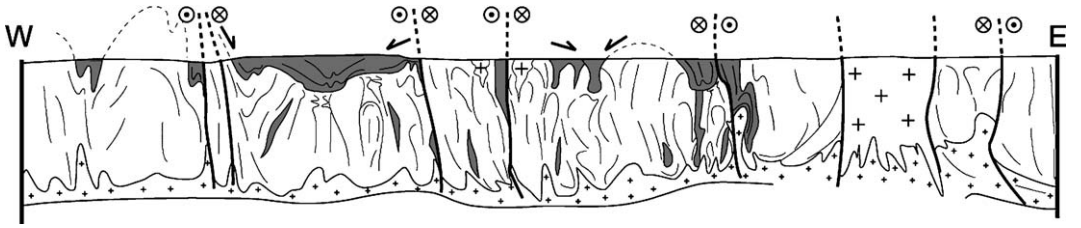

Fig. 14. Example of interpretative crustal-scale cross-section through an Archaean granite–greenstone transpressive belt (Dharwar Craton, India). Bottom line is the Moho; steeply dipping lines are foliation traces and shear zones; grey areas are greenstones; crossed areas are granitic domains. Modified after Chardon et al., 1998.

marked by regional-scale steeply dipping foliations, and (2) vertical burial of upper-crustal domains. In Archaean deformation zones, the association between gneiss domes and greenstone belts is commonly attributed to vertical motions involving sagduction of dense upper crustal material within underlying partially melted continental crust (e.g. Gorman et al., 1978; Schwerdtner and Lumbers, 1980; Goodwin and Smith, 1980; Dixon and Summers, 1983; Bouhallier et al., 1995; Choukroune et al., 1995; Chardon et al., 1996; Choukroune et al., 1997; Collins et al., 1998). The important role of diapirism in the upward motion of hot and buoyant gneiss domes has also been invoked in Paleoproterozoic (Brun et al., 1981; Bleeker and Westra, 1987; Pons et al., 1995; Caby et al., 2000), and up to Neoproterozoic times (Hippertt and Davis, 2000). Most of these interpretations consider that vertical motions are driven by inverse density profiles, while the possible role of plate boundary tectonic forces is often neglected. A major outcome of our experiments is that compression of a weak lithosphere results in downward motion of upper-crustal pop downs accommodated by thrusting without requiring any inverse density profile.

Associations of thrust faulting and granite–greenstone belts have been described in several natural examples (Gorman et al., 1978; Sawyer and Benn, 1993; Camiré and Burg, 1993; Choukroune et al., 1997; Griffin et al., 2004). Granite–greenstone belts are generally associated with high-grade metamorphism and are affected by intense distributed horizontal shortening (e.g. Chardon et al., 1998) (Fig. 14). Therefore, deformation patterns mainly reflect late evolution stages where supracrustal rocks are ductile because substantially buried in the crust. Interfaces between gneiss domes and greenstones are thus generally steeply dipping and marked by intense shearing deformations that attest to relative vertical motions (Fig. 14). Nevertheless, moderately deformed greenstone belts may appear to be bounded by normal faults (e.g. Bababudan belt, Darwar Craton, Fig. 14), which suggests that local inverse density profiles may have some control on sites of preferred onset of sagduction.

Models emphasize that compression of weak and dominantly ductile lithospheres should result in distributed thickening, thrusts being limited to the thin upper brittle crust. However, the observed strain pattern indicates that the zones of pop down stacking could further trigger strain localisation within vertical deformation zones associated with vertical stretch. Many ancient deformation belts are marked by distributed thickening, but also by vertical transpressive zones that accommodate important components of vertical stretch (Hudleston et al., 1988; Bouhallier et al., 1995; Chardon et al., 1998; Lonka et al., 1998; Gapais et al., 2005) (Fig. 14). These belts are also characterized by the juxtaposition, at the same structural level, of buried supracrustals and basement-dominated domains. Supracrustals may be dominated by dense rocks, as in Archaean greenstones, but also by metasediments, as observed in some Proterozoic belts (e.g. Coats et al., 1972; Simonen, 1980; Ehlers et al., 1986). In most examples, deformations are marked by important synkinematic magmatism and by widespread HT–LP metamorphic signatures (e.g. Sandiford, 1989; Bleeker, 1990; Ehlers et al., 1993; Percival, 1994 and refs. therein; Monnier et al., 1996; Holzer et al., 1999; Caby et al., 2000; Vassallo and Wilson, 2002) consistent with overall hot and weak lithospheres (e.g. Bailey, 1999; Cheng et al., 2002; Rey et al., 2003). As in our models, most of these peculiar deformation belts show poor evidence for large-scale thrust and nappe tectonics. Thus, metamorphic conditions are often monotonous over large surfaces, suggesting that isotherms remained rather flat despite intense horizontal shortening and crustal thickening (e.g. Ehlers et al., 1993; Pelletier et al., 2002; Gapais et al., 2005). This latter feature is consistent with strain patterns developed in our models, where the overall envelopes of initially horizontal markers remain flat after 50% shortening. A broadly distributed deformation throughout the ductile lithosphere is further

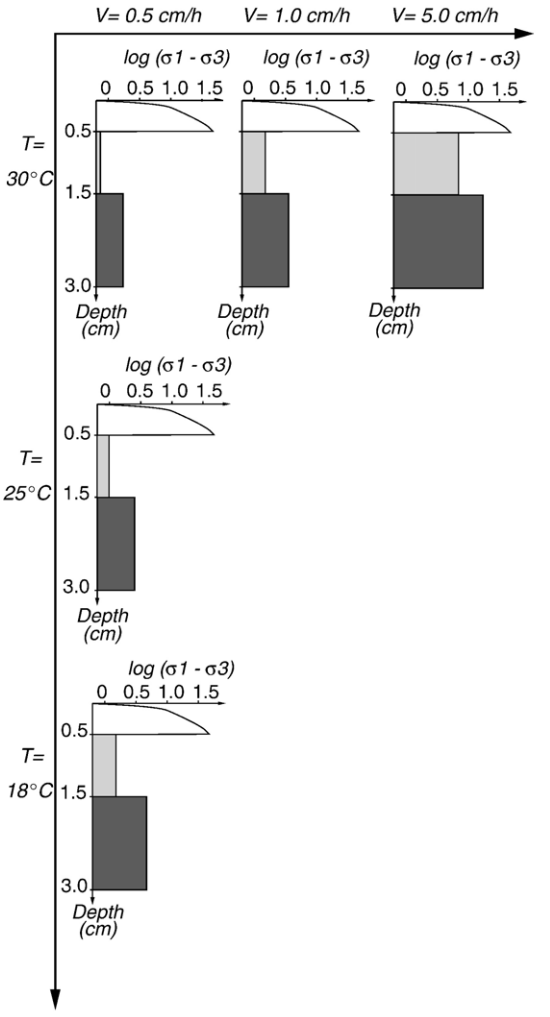

Temperature T (°C)	Velocity V (cm/h)	σ1 - σ3 (Pa)	
		ductile crust	ductile mantle
30	5.0	0.74	1.71
	1.0	1.48	3.42
	0.5	7.04	17.12
25	0.5	0.92	2.54
18	0.5	1.53	4.62

Fig. 15. Estimates of strength profiles for the series of experiments at different convergence rates (boundary velocities) and temperatures. Table gives strength values.

expected to favour limited isostatic disequilibrium, and consequently distributed and preferentially limited topographic gradients. This is supported by analogue models (Davy and Cobbold, 1991) (Figs. 1 and 4), as well as by thermal models involving hot lithospheres (Rey et al., 2001b; Rey and Houseman, in press).

4.3. Implications for high-plateaus

Beside implications for ancient deformation zones involving juvenile terrains, one may consider thickened and thermally re-equilibrated lithospheres, as for example expected below High Plateaus like the Altiplano or Tibet. There, many lines of evidence suggest that the crust is thick and hot, probably marked by partially melted zones below 20 km (see Dewey et al., 1988; Wigger et al., 1994; Nelson et al., 1996; Schwartz and Krüger, 1997; Hacker et al., 2000; Yuan et al., 2000; Ducea et al., 2003). Below the Andean Altiplano, geophysical data indicate that compressive deformations currently occur, while surface geology suggests moderate erosion and deformation of the upper crust since the last 10 Ma (Lamb et al., 1997).

In the Tibet plateau where crustal thickness is around 65±5 km (Zhao et al., 2001), seismic estimates of the α−β quartz transition indicate temperatures of 700 °C at 18 km depth and 800 °C at 32 km (Mechie et al., 2004) confirming previous indicators for a hot crust (Nelson et al., 1996; Hacker et al., 2000; Wei et al., 2001; Ducea et al., 2003). At moderate wavelengths of approximately 100 km, the plateau is flat with relief of approximately 1 km or less for most of Tibet, as opposed to the much higher relief of up to 6 km on the plateau edges (Fielding et al., 1994). Thin plate flexure modelling reveals lateral variations of the elastic thickness (Te) around low values, in the bound 10–30 km, in most of the Tibet plateau and with lower values in the Qiantang terrain, where Te reaches 8 km (Braitenberg et al., 2003). Such flatness and low Te values for a thick crust provide strong arguments in favour of crust weakness. The large-scale morphology of eastern Tibet reflects fluid flow within the underlying crust whose modelling suggests low viscosities from 10^{18} Pas beneath the plateau margins to an upper bound of 10^{16} Pas beneath the plateau (Clark and Royden, 2000). As has been shown long ago, the surface geology in central Tibet does not bring evidence for strong crustal shortening (Kidd et al., 1988; Burg et al., 1994; Coward et al., 1998) despite a crustal thickness around 65 km. Deformation is distributed with no clear vergence of thrusts and no significant hangingwall topography (Fielding et al., 1994; Fielding, 1996; Murphy et al., 1997; Kapp et al., 2005). Seismic evidence suggests that convergence has been largely accommodated through pure-shear thickening accompanied by removal of lower crustal material by lateral ductile flow (Haines et al.,

2003). GPS data (Zhang et al., 2004) also argue for distributed deformations across the plateau, still accummulating today, and demonstrate a transverse shortening velocity component of 2 cm/y between the Tsangpo suture zone and the northern border of the plateau — i.e. 20 km of shortening per million of years.

The above lines of evidence all indicate that the Tibet plateau corresponds to a hot and weak crust that was and is still thickening by distributed shortening. Such thickening likely corresponds to pure shear at lithosphere scale ("vertical plane strain NS shortening" of Dewey et al., 1988) and, as illustrated in our experiments, could operate by pop-down thrusting of the brittle upper crust and ductile flow of the underlying crust and mantle. Finally, the pop-down mode of upper crust deformation offers a simple solution to the tectonic paradox of High Plateaus of Tibet-type where the crust is significantly thickened without neither significant topographic gradients nor evidence of strong shortening at surface.

5. Conclusions

The analogue modelling study of weak lithosphere shortening presented in this paper emphasizes an original mode of thickening that can be summarised as follows.

1. The whole lithosphere undergoes nearly vertical pure shear with the envelopes of surface, Moho and lithosphere base remaining close to horizontal, even for strong amounts of bulk shortening.
2. Thrusting that is limited to the brittle upper crust results in burial of "pop-down" units. The number of simultaneous pop-down units reduces with decreasing values of mechanical coupling between brittle and ductile layers. Shortening absorbed at a restricted number of sites leads to the stacking of several pop-down units.
3. Horizontal shortening results in distributed thickening of crust and mantle ductile layers.

Such mode of lithosphere thickening, where pieces of the upper crust are pop-down into the ductile crust without inverse density profile, sheds new light on the followings.

4. The overall deformation pattern of ancient deformation zones involving juvenile crust, as commonly observed in Archaean and Paleoproterozoic times.
5. The tectonic paradox of High Plateaus of Tibet-type where the crust is significantly thickened without neither significant topographic gradients nor evidence of strong shortening at surface.

Acknowledgements

This paper is a contribution of a CNRS program (DyETI). J-P Brun acknowledges financial support from the Institut Universitaire de France. We thank J.J. Kermarrec, N. Durrieu, N. Carry and S. Schueller for their help in the modelling laboratory and P. Rey and an anonymous referee for suggestions of improvements and constructive remarks.

Appendix A. Strength profiles

In the sand layer, the critical stress can be expressed in terms of the difference between maximum and minimum principal stresses and material parameters (Ranalli, 2000). For thrust fault,

$$\sigma 1 - \sigma 3 = [2\mu\rho g z(1-\lambda) + 2S]/[(\mu^2+1)^{1/2} - \mu], \qquad (1)$$

where μ is the frictional coefficient with a mean value of 0.58 (Krantz, 1991; Martinod, 1991); ρ is the density of the sand; g is the acceleration due to the gravity; z is the thickness of the sand layer; λ is the pore fluid factor (here equal to zero); S is the cohesion factor of the material (equal to zero in our experiments, because the cohesion of Fontainebleau sand used is negligible).

In the silicone layers, the shear stress is:

$$\tau = \mu V / t_s, \qquad (2)$$

where t_s and μ correspond to the length and the viscosity of the silicone layer, respectively, and V is the velocity of horizontal displacement at the onset of the experiment.

Fig. 15 shows the theoretical strength profiles calculated for models done at different displacement velocities (V) and temperatures (T). Decrease in temperature and (or) increase in velocity induce strengthening of model lithospheres. Thus, the series of experiments (Table 1) allowed us to investigate the effects of the variations of strength profiles on deformation modes.

References

Bailey, R.C., 1999. Gravity-driven continental overflow and Archaean tectonics. Nature 398, 413–415.

Beaumont, C., Ellis, S., Hamilton, J., Fullsack, P., 1996. Mechanical model for subduction–collision tectonics of Alpine-type compressional orogens. Geology 24, 675–678.

Bleeker, W., 1990. New structural–metamorphic constraints on Early Proterozoic oblique collision along the Thompson Nickel Belt, Manitoba. Geol. Assoc. Can. Spec. Pap. 37, 57–73.

Bleeker, W., Westra, L., 1987. The evolution of the Mustio gneiss dome, Svecofennides of SW Finlan. Precambrian Res. 36, 227–240.

Bouhallier, H., Chardon, D., Choukroune, P., 1995. Strain patterns in Archaean dome and basin structures: the Darwar craton (Karnakata South India). Earth. Planet. Sci. Lett. 135, 57–75.

Braitenberg, C., Wang, Y., Fang, J., Hsu, H.T., 2003. Spatial variations of flexure parameters over the Tibet–Quinghai plateau. Earth. Planet. Sci. Lett. 205 (3–4), 211–224.

Braun, J., Pauselli, C., 2004. Tectonic evolution of the Lachlan Fold Belt, southeastern Australia: constraints from coupled numerical models of crustal deformation and surface erosion driven by subduction of the underlying mantle. Phys. Earth Planet. Inter. 141 (4), 281–301.

Brun, J.P., 1999. Narrow rifts vs. wide rifts: inferences for the mechanics of rifting for laboratory experiments. Philos. Trans. R. Soc. Lond., A 357, 695–712.

Brun, J.P., 2002. Deformation of the continental lithosphere: insights from brittle–ductile model. In: De Meers, S., Drury, M.R., De Bresser, J.H.P., Pennock, G.M. (Eds.), Deformation Mechanisms, Rheology and Tectonics: Current Status and Future Perspectives-Geol. Soc. London Spec. Pub., vol. 200, pp. 355–370.

Brun, J.P., Fort, X., 2004. Compressional salt tectonics (Angolan margin). Tectonophysics 382, 129–150.

Brun, J.P., Gapais, D., Le Theoff, B., 1981. The mantled gneiss domes of Kuopio (Finland): interfering diapirs. Tectonophysics 74, 283–304.

Burg, J.P., Davy, P., Martinod, J., 1994. Shortening of analogue models of the continental lithosphere: new hypothesis for the formation of the Tibetan plateau. Tectonics 13 (2), 475–483.

Caby, R., Delor, C., Agoh, O., 2000. Lithologie, structure et métamorphisme des formations birimiennes dans la région d'Odienné (Côte d'Ivoire) : rôle majeur du diapirisme des plutons et des décrochements en bordure du craton de Man. J. Afr. Earth Sci. 30, 351–374.

Camiré, G.E., Burg, J.P., 1993. Late Archaean thrusting in the northwestern Pontiac Subprovince, Canadian Shield. Precambrian Res. 61, 51–66.

Chardon, D., Choukroune, P., Jayananda, M., 1996. Strain patterns, décollement and incipient sagducted greenstone terrains in south India. J. Struct. Geol. 18, 991–1004.

Chardon, D., Choukroune, P., Jayananda, M., 1998. Sinking of the Dharwar Basin (south India): implications for Archaean tectonics. Precambrian Res. 91 (1–2), 15–39.

Cheng, L.Z., Mareschal, J., Jaupart, C., Rolandone, F., Gariepyand, C., Radigon, M., 2002. Simultaneous inversion of gravity and heat flow data: constraints on thermal regime, rheology and evolution of the Canadian Shield crust. J. Geodyn. 34, 11–30.

Choukroune, P., 1989. The ECORS Pyrenean deep seismic profile reflection data and the overall structure of the orogenic belt. Tectonics 8, 23–39.

Choukroune, P., Roure, F., Pinet, B., ECORS Pyrenees Team, 1990. Main results of the ECORS Pyrenees profile. Tectonophysics 173, 411–423.

Choukroune, P., Bouhallier, H., Arndt, N.T., 1995. Soft lithosphere during periods of Archean crustal growth or crustal reworking. In: Coward, M.P., Riess, A.C. (Eds.), Early Precambrian Processes-Geol. Soc. London. Spec. Pub., vol. 95, pp. 67–86.

Choukroune, P., Ludden, J.N., Chardon, D., Calvert, A.J., Bouhallier, H., 1997. Archean crustal growth and tectonic processes: a comparison of the Superior province, Canada and the Dharwar Craton, India. In: Burg, J.P., Ford, M. (Eds.), Orogeny Through Time. Geol. Soc. London. Spec. Pub., vol. 121, pp. 63–98.

Clark, M.K., Royden, L., 2000. Topographic ooze: building the eastern margin of Tibet by lower crustal flow. Geology 28, 703–706.

Coats, C.J.A., Quirke, J.R., Bell, T.T., Cranstone, D.A., Campbell, F.H.A., 1972. Geology and mineral deposits of the Flin Flon, Lynn Lake and Thompson areas, Manitoba and the Churchil Superior Front of the Western Precambrian Shield. Field Excursion Guidebook, 24th International Geological Congress, pp. A31–C31.

Cobbold, P.R., Davy, P., Gapais, D., Rossello, E.A., Sadybakasov, E., Thomas, J.C., Tondji Biyo, J.J., De Urreiztieta, M., 1993. Sedimentary basins and crustal thickening. Sediment. Geol. 86 (1–2), 77–89.

Collins, W.J., 2002. Hot orogens, tectonic switching and creation of continental crust. Geology 30 (6), 535–538.

Collins, W.J., Van Kranendonk, M.J., Teyssier, C., 1998. Partial convective overturn of Archean crust in the east Pilbara Craton, western Australia: driving mechanisms and tectonic implications. J. Struct. Geol. 20, 1405–1424.

Coward, M.P., Kidd, W.S.F., Pan, Y., Shackleton, R.M., Zhang, H., 1998. The structure of the 1985 Tibet Geotraverse, Lhasa to Golmud. Philos. Trans. R. Soc. Lond., A 327, 307–336.

Davy, P., Cobbold, P.R., 1991. Experiments on shortening of a 4-layer model of the continental lithosphere. Tectonophysics 188, 1–25.

Davy, P., Choukroune, P., Suzanne, P., 1990. Hypothèses mécaniques de déformation de la lithosphère appliquées à la formation des Pyrénées. Bull. Soc. Geol. Fr. 8, 219–228.

Dewey, J.F., Shackleton, R.M., Chengfa, C., Yiyin, S., 1988. The tectonic evolution of the Tibetan Plateau. Philos. Trans. R. Soc. Lond., A 327, 379–413.

De Wit, M.J., 1998. On Archean granites, greenstones, cratons and teconics: does the evidence demand a verdict? Precambrian Res 91 (1–2), 181–226.

Dixon, J.M., Summers, J.M., 1983. Patterns of total and incremental strain in subsiding troughs: experimental centrifuged models of inter-diapir synclines. Can. J. Earth Sci. 20, 1843–1861.

Ducea, M.N., Lutkov, V., Minaev, V.T., Hacker, B., Ratschbacher, L., Luffi, P., Schwab, M., Gehrels, G.E., McWilliams, M., Vervoort, J., Metcalf, J., 2003. Building the Pamirs: the view from the underside. Geology 31 (10), 849–852, doi:10.1130/G19707.1.

Ehlers, C., Lindros, A., Jaanus-Järkkälä, M., 1986. Stratigraphy and geochemistry in the Proterozoic mafic volcanic rocks of the Nagu–Korpo area, SW Finland. Precambrian Res. 32, 297–315.

Ehlers, C., Lindros, A., Selonen, O., 1993. The late-Svecofenian granite–migmatite zone of southern Finland — a belt of transpressive deformation and granite emplacement. Precambrian Res. 64, 295–309.

England, P.C., McKenzie, D.P., 1982. A thin viscous sheet model for continental deformation. Geophys. J. R. Astron. Soc. 70, 295–321.

Fielding, E., 1996. Tibet uplift and erosion. Tectonophysics 260 (1–3), 55–84.

Fielding, E., Isacks, B., Barazangi, M., Duncan, C., 1994. How flat is Tibet? Geology 22 (2), 163–167.

Fort, X., Brun, J.P., Chauvel, F., 2004. Salt tectonics on the Angolan margin, synsedimentary deformation processes. AAPG Bull. 88 (11), 1523–1544.

Gapais, D., Potrel, A., Machado, N., Hallot, E., 2005. Kinematics of long-lasting Paleoproterozoic transpression within the Thompson Nickel Belt (Manitoba, Canada). Tectonics 24, 1–16.

Goodwin, A.M., Smith, I.E.M., 1980. Chemical discontinuities in Archean volcanic terrains and the development of Archean crust. Precambrian Res. 10, 301–311.

Gorman, B.E., Pearce, T.H., Birkett, T.C., 1978. On the structure of Archean greenstone belts. Precambrian Res. 6, 23–41.

Griffin, W.L., Belousova, E.A., Shee, S.R., Pearson, N.J., O'Reilly, S.Y., 2004. Archean crustal evolution in the northern Yilgarn Craton: U–Pb and Hf-isotope evidence from detrital zircons. Precambrian Res. 131, 231–282.

Hacker, B.R., Gnos, E., Ratschbacher, L., Grove, M., McWilliams, M., Sobolev, S.V., Jiang, W., Wu, Z., 2000. Hot and dry deep crustal xenoliths from Tibet. Science 287, 2463–2466.

Haines, S.S., Klemperer, S.L., Brown, L., Guo, J., Mechie, J., Meissner, R., Ross, A., Wenjin, Z., 2003. INDEPTH III seismic data: from surface observations to deep crustal processes in Tibet. Tectonics 22, 1001, doi:10.1029/2001TC001305.

Hamilton, W.B., 1998. Archean magmatism and deformation were not products of plate tectonics. Precambrian Res. 91 (1–2), 143–179.

Hamilton, W.B., 2003. An alternative Earth. GSA Today 13, 4–12.

Harrison, T.M., Grove, M., Lovera, O.M., Catlos, E., 1998. A model for the origin of Himalayan anatexis and inverted metamorphism. J. Geophys. Res. 103, 27017–27032.

Hauck, M.L., Nelson, K.D., Brown, L.D., Zhao, W., Ross, A.R., 1988. Crustal structure of the Himalayan orogen at ~90° east longitude from project INDEPTH deep reflection profiles. Tectonics 17, 481–500.

Hippertt, J., Davis, B., 2000. Dome emplacement and formation of kilometre-scale synclines in a granite–greenstone terrain (Quadrilatero Ferrifero, southeastern Brazil). Precambrian Res. 102, 99–121.

Holzer, L., Barton, J.M., Paya, B.K., Kramers, J.D., 1999. Tectonothermal history of the western part of the Limpopo Belt: tectonic models and new perspectives. J. Afr. Earth Sci. 28, 383–402.

Houseman, G.A., Molnar, P., 1997. Gravitational (Rayleigh–Taylor) instability of a layer with non-linear viscosity and convective thinning of continental lithosphere. Geophys. J. Int. 128, 125–150.

Hudleston, P.J., Schultz-Ela, D., Southwick, D.L., 1988. Transpression in an Archean greenstone belt, northern Minnesota. Can. J. Earth Sci. 25, 1060–1068.

Hyndman, R.D., Currie, C.A., Mazzotti, S.P., 2005. Subduction zone backarcs, mobile belts, and orogenic heat. GSA Today 15 (2), 4–10.

Jackson, M.P.A., Talbot, C.J., 1994. Advances in salt tectonics. In: Hancock, P. (Ed.), Continental Deformation. Pergamon Press, Oxford, pp. 159–179.

Kapp, P., Yin, A., Harrison, T.M., Ding, L., 2005. Cretaceous–Tertiary shortening, basin development, and volcanism in central Tibet. Geol. Soc. Amer. Bull. 117, 865–878.

Kidd, W.S.F., Yusheng, P., Chengfa, C., Coward, M.P., Dewey, J.F., Gansser, A., Molnar, P., Shackleton, R.M., Yiyin, F.R.S., 1988. Geological mapping of the 1985 Chinese–British Tibetan (Xizang–Qinghai) Plateau Geotraverse route. Philos. Trans. R. Soc. Lond., A 327, 287–305.

Krantz, R.W., 1991. Measurements of friction coefficients and cohesion for faulting and fault reactivation in laboratory models using sand and sand mixtures. Tectonophysics 188, 203–207.

Lamb, S., Hoke, L., Kennan, L., Dewey, J., 1997. Cenozoic evolution of the central Andes in Bolivia and northern Chile. In: Burg, J.P., Ford, M. (Eds.), Orogeny Through Time. Geol. Soc. London. Spec. Pub., vol. 121, pp. 237–264.

Lonka, H., Schulmann, K., Venera, Z., 1998. Ductile deformation of tonalite in the Suomusjarvi shear zone, south-western Finland. J. Struct. Geol. 20, 783–798.

Malavieille, J., 1984. Modélisation expérimentale des chevauchements imbriqués: Application aux chaines de montagnes. Bull. Soc. Geol. Fr. 7, 129–138.

Martinod, J., 1991. Instabilités périodiques de la lithosphère (flambage, boudinage), en compression et en extension. Mem. Doc. Cent. Armor. Etud. Struct. Socles, Rennes 44, 283.

McClelland, W.C., Oldow, J.S., 2004. Displacement transfer between thick- and thin-skinned décollement systems in central North American Cordillera. In: Grocott, J., McCaffrey, K.J.W., Taylor, G., Tikoff, B. (Eds.), Vertical coupling and decoupling in the lithosphere. Geol. Soc. Lond. Spe. Pub., vol. 227, pp. 177–195.

Mechie, J., Sobolev, S.V., Ratschbacher, L., Babeyko, A.Y., Bock, G., Jones, A.G., Nelson, K.D., Solon, K.D., Brown, L.D., Zhao, W., 2004. Precise temperature estimation in the Tibetan crust from seismic detection of the α–β quartz transition. Geology 32, 601–604.

Monnier, O., Ménot, R.P., Peucat, J.J., Fanning, M., Giret, A., 1996. Actualisation des données géologiques sue Terre Adélie (Antartique est): mise en évidence d'un collage tectonique au Protérozoïque. C.R. Acad. Sci. Paris, Série D 322, 55–62.

Murphy, M.A., Yin, A., Harrison, T.M., Dürr, S.B., Chen, Z., Ryerson, F.J., Kidd, W.S.F., Wang, X., Zhou, X., 1997. Did the Indo-Asian collision alone create the Tibetan plateau? Geology 25, 719–722.

Nelson, K.D., Zhao, W., Brown, L.D., Kuo, J., Che, J., Liu, X., Klemperer, S.L., Makovsky, Y., Meissner, R., Mechie, J., Kind, R., Wenzel, F., Ni, J., Nabelek, J., Leshou, C., Tan, H., Wei, W., Jones, A.G., Booker, J., Unsworth, M., Kidd, W.S.F., Hauck, M., Alsdorf, D., Ross, A., Cogan, M., Wu, C., Sandvol, E., Edwards, M., 1996. Partially molten middle crust beneath southern Tibet: synthesis of project INDEPTH results. Science 274 (5293), 1684–1688.

Pelletier, A., Gapais, D., Ménot, R.P., Peucat, J.J., 2002. Tectonique transpressive en Terre Adélie (est Antartique). Comptes Rendus. Geosci. 334, 505–511.

Percival, J.A., 1994. Archean high-grade metamorphism. In: Condie, K.C. (Ed.), Archean Crustal Evolution. Elsevier, Amsterdam, pp. 357–410.

Pfiffner, A., Ellis, S., Beaumont, C., 2000. Collision tectonics in the Swiss Alps from geodynamic modelling. Tectonics 19, 1065–1094.

Pons, J., Barbey, P., Dupuis, D., Léger, J.M., 1995. Mechanisms of pluton emplacement and structural evolution of the 2.1 Ga juvenile continental crust: the Birimien of southwestern Niger. Precambrian Res. 70, 281–305.

Ranalli, G., 1997. Rheology of the lithosphere in space and time. In: Burg, J.P., Ford, M. (Eds.), Orogeny Through Time. Geol. Soc. Lond. Spe. Pub., vol. 121, pp. 19–37.

Ranalli, G., 2000. Rheology of the crust and its role in tectonic reactivation. J. Geodyn. 30, 3–15.

Rey, P.F. Houseman, G., in press. Lithospheric scale gravitational flow: the impact of body forces on orogenic processes from Archaean to Phanaerozoic. In: Buiter, S., Schreurs, G. (Eds.), Analogue and Numerical Modelling of Crustal-Scale Processes. Geol. Soc. Lond. Spec. Pub.

Rey, P., Vanderhaeghe, O., Teyssier, C., 2001a. Gravitational collapse of the continental crust: definition, regimes and modes. Tectonophysics 342 (3–4), 435–449.

Rey, P.F., Houseman, G., Poudjom Djomani, Y.H., Griffin, W.L., O'Reilly, S.Y., 2001b. The impact of body forces on Archaean continental lithosphere. 4IAS conference (Perth WA). AGSO Geosci. Aust. Rec. 37, 84–86.

Rey, P.F., Philippot, P., Thébaud, N., 2003. Contribution of mantle plumes, crustal thickening and greenstone blanketing to the 2.75–2.65 Ga global crisis. Precambrian Res. 127, 43–60.

Roure, F., Choukroune, P., Berastegui, X., Munoz, J.A., Villien, A., Matheron, P., Bareyt, M., Séguret, M., Camara, P., Déramond, J., 1989. ECORS deep seismic data and balanced cross-sections; geometric constraints on the evolution of the Pyrenees. Tectonics 8, 41–50.

Sandiford, M., 1989. Secular trends in the thermal evolution of metamorphic terrains. Earth Planet. Sci. Lett. 95, 85–96.

Sawyer, E.W., Benn, K., 1993. Structure of the high-grade Opatica belt and adjacent low-grade Abitibi subprovince and Archaean mountain front. J. Struct. Geol. 15, 1443–1458.

Schmid, S.M., Kissling, E., 2000. The arc of the western Alps in the light of new data on deep crustal structure. Tectonics 19, 62–85.

Schmid, S.M., Fügenschuh, B., Kissling, E., Schuster, R., 2004. Tectonic map and overall architecture of the Alpine orogen. Eclogae Geol. Helv. 97, 93–117.

Schwartz, G., Krüger, D., 1997. Resistivity cross section through the southern central Andes as inferred from magnetotelluric and geomagnetic deep soundings. J. Geophys. Res. 102 (B6), 11957–11978.

Schwerdtner, W.M., Lumbers, S.B., 1980. Major diapiric structures in the Superior and Greenville provinces of the Canadian Shield. Geol. Assoc. Can. Spec. Pap. 20, 149–180.

Simonen, A., 1980. The Precambrian in Finland. Geol. Surv. Finland 304. 58 pp.

Sonder, L.J., England, P.C., Wernicke, B.P., Christiansen, R.L., 1987. A physical model for Cenozoic extension of western North America. In: Coward, M.P., Dewey, J.F., Hancocks, P.L. (Eds.), Continental Extension Tectonics. Geol. Soc. Lond. Spe. Pub., vol. 28, pp. 187–201.

Vassallo, J.J., Wilson, C.J.L., 2002. Palaeoproterozoic regional-scale non-coaxial deformation: an example from eastern Eyre Peninsula, south Australia. J. Struct. Geol. 24, 1–24.

Wakabayashi, J., 2004. Tectonic mechanisms associated with *P–T* paths of regional metamorphism: alternatives to single-cycle thrusting and heating. Tectonophysics 392, 193–218.

Wei, W., Unsworth, M., Jones, A., Booker, J., Tan, H., Nelson, D., Chen, L., Li, S., Solon, K., Bedrosian, P., Jin, S., Ledo, J., Kay, D., Roberts, B., 2001. Detection of widespread fluids in the Tibetan crust by magnetotelluric studies. Science 292, 716–718.

Wigger, P.J., Schmitz, M., Araneda, M., Asch, G., Baldzuhn, S., Giese, P., Heinsohn, W.D., Martinez, E., Ricaldi, E., Röwer, P., Viramonte, J., 1994. Variation in the structure of the southern central Andes deduced from seismic refraction investigations. In: Reuters, K.J., Scheuber, E., Wigger, P.J. (Eds.), Tectonics of the Southern Central Andes. Structure and Evolution of an Active Continental Margin. Springer-Verlag, Berlin, pp. 23–48.

Windley, B.F., 1993. Uniformitarian today: plate tectonics is the key to the past. J. Geol. Soc. 150 (1), 7–19.

Yuan, X., Sobolev, S.V., Kind, R., Oncken, O., Bock, G., Ash, G., Schurr, B., Graeber, F., Rudloff, A., Hanka, A., 2000. Subduction and collision processes in the central Andes constrained by converted seismic phases. Nature 408, 958–961.

Zhang, P.Z., Shen, Z., Wang, M., Gan, W., Bürgmann, R., Molnar, P., Wang, Q., Niu, Z., Sun, J., Wu, J., Hanrong, S., Xinzhao, Y., 2004. Continuous deformation of the Tibetan Plateau from global positioning system data. Geology 32, 809–812.

Zhao, W., Mechie, J., Brown, L.D., Guo, J., Haines, S., Hearn, T., Klemperer, S.L., Ma, Y.S., Meissner, R., Nelson, K.D., Ni, J.F., Pananont, P., Rapine, R., Ross, A., Saul, J., 2001. Crustal structure of central Tibet as derived from project INDEPTH wide-angle seismic data. Geophys. J. Int. 145, 486–498.